หนึ่งผลงานหนึ่งอาจารย์

IP Router Using Optical Address Recognition with Second-Harmonic Generator*

Assoc. Prof. Dr. Joewono Widjaja

สาขาวิชาเทคโนโลยีเลเซอร์และโฟตอนนิกส์

สำนักวิชาวิทยาศาสตร์

มีนาคม 2546

---

*This is a substitute for the original project that is still on progress.

Contents

pages 1237–1298 10th October 2002 Vol. 38 No. 21

(continued overleaf)

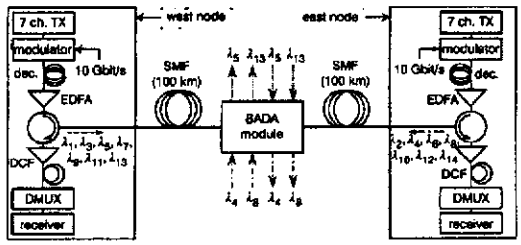

Fig. 2 *Experimental setup with implemented BADA module*

Fig. 3*a* shows the measured BER curves of the dropped and the added signals at the BADA module. The receiver sensitivity was slightly improved owing to the pulse compression by the chirping of the modulator. We also show the BER curves of the signals passed through the BADA module, Fig. 3*b*. The measured sensitivity penalty at a BER of 10^{-10} was <0.5 dB.

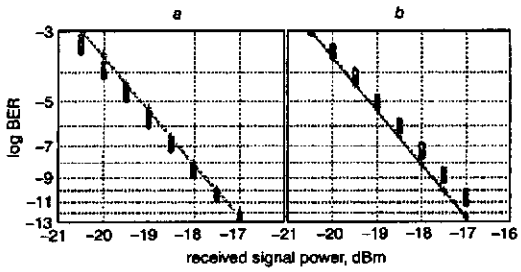

Fig. 3 *Measured BER curves*

a Add/drop signals (transmission distance: 100 km)
b Pass-through signals (transmission distance: 200 km)

Discussion: To estimate the scalability of the BADA module, we calculated the power penalty caused by the accumulation of the RINs, as shown in Fig. 4 [4]. We used the actual component parameters and the resultant penalty at a BER of 10^{-10} was <0.2 dB even when the signals pass through 10 modules.

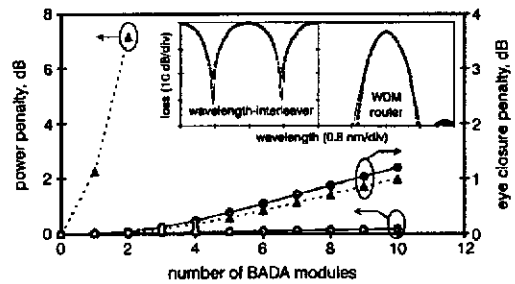

Fig. 4 *RIN-induced power penalty and eye closure penalty in a function of cascaded BADA modules*

• with wavelength-interleavers (original architecture)
▲ with circulators instead of wavelength-interleavers
Insets: Measured and modelled spectral responses of wavelength-interleaver and router

Compared with the conventional add/drop multiplexers [1] and the previous BADA modules [2–3], the BADA module further comprises wavelength-interleavers. They could suppress the RINs more effectively than the circulators as shown in Fig. 4. However, they reduce the effective bandwidth of the signal path and can consequently cause extra signal distortion. We carried out numerical simulations to investigate this effect and show the resultant eye closure penalty in Fig. 4. We modelled the WDM router as a Gaussin filter and the wavelength-interleaver as a Mach-Zehnder interferometer filter, which agreed well with the measured data as shown in the insets of Fig. 4. The extra eye closure penalty caused by the wavelength-interleavers was <0.2 dB even when 10 BADA modules were cascaded. It may be noted that the overall eye closure penalty will decrease if we use WDM routers with flat-top passbands.

To evaluate the performance of the BADA module in detail, we measured BERs by replacing the BADA module in Fig. 2 into a uni-directional amplifier with identical gain and noise figure. We kept other transmission conditions unchanged. Fig. 5 shows the receiver sensitivities at a BER of 10^{-10} after transmission over 200 km of SMF. The sensitivity penalty of the bi-directional transmission was <0.3 dB even in the worst-case channel. It was close to the theoretical estimation of 0.2 dB.

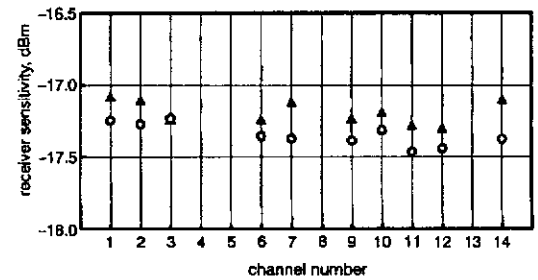

Fig. 5 *Measured receiver sensitivities after transmission over 200 km SMF*

▲ bi-directional transmission with BADA module
• uni-directional transmission with uni-directional amplifier

Conclusion: We have demonstrated a cost-effective BADA for use in high-capacity bi-directional WDM networks. The BADA module consists of only one $N \times N$ WDM router and one DCF module. The sensitivity penalty compared with uni-directional transmission was <0.3 dB when we used the module in a 14×10 Gbit/s bi-directional transmission over 200 km of SMF.

2 April 2002
Electronics Letters Online No: 20020849
DOI: 10.1049/el:20020849

Hyun Deok Kim, Jeong-Hun Shin and Chang-Hee Lee (*Department of EECS, Korea Advanced Institute of Science and Technology, 373-1, Kusong-dong, Yusong-gu Taejon 305-701, Korea*)

E-mail: chl@ee.kaist.ac.kr

References

1 ELREFAIE, A.F.: 'Multiwavelength survivable ring network architectures', Int. Conf. Communication'93, Paper 48.7, Vol. 2, Paper 48.7, pp. 1245–1251
2 KIM, C.H., LEE, C.-H., and CHUNG, Y.C.: 'Bi-directional WDM self-healing ring network based on simple bi-directional add/drop amplifier modules', *IEEE Photonics Technol. Lett.*, 1998, **10**, (9), pp. 1340–1342
3 SHIN, J.-H., KIM, H.D., CHO, Y., SHIM, C.S., and LEE, C.-H.: 'Demonstration of self-healing and automatic retrieval in a two-fibre bi-directional WDM ring network', *Electron. Lett.*, 1998, **37**, (3), pp. 188–190
4 GIMLETT, J.L., IQBAL, M.Z., CURTIS, L., CHEUNG, N.K., RIGHETTI, A., FONTANA, F., and GRASSO, G.: 'Impact of multiple reflection noise in Gbit/s lightwave systems with optical fibre amplifiers', *Electron. Lett.*, 1989, **25**, (20), pp. 1393–1394
5 KIM, H.D., SHIN, J.-H., HWANG, S.-T., OH, Y.J., and LEE, C.-H.: 'Bi-directional add/drop amplifier module with a single dispersion compensating fiber module'. OFC'2001, Anaheim, CA, USA, March 2001, Paper WH2

IP router using optical address recognition with second-harmonic generator

J. Widjaja

A novel optical header address recognition using a second-harmonic generator cascaded with optical correlator is proposed as a cost-effective way of realising routing in optical networks. The second-harmonic generator is used for minimising optical loss due to wavelength mismatch, while the optical correlator performs address recognition.

Introduction: We recently proposed a novel architecture for implementing an IP router using a holographic header address processor [1]. Our method takes advantage of an inherent parallelism of optics together with the low cost and huge storage capacity of the angular-multiplexed hologram. This is accomplished by first encoding each IP header address onto an optical code generated from a modelocked laser diode operating at a wavelength of 1550 nm. Using a diffraction grating to convert temporal information of the optically encoded address into a spatial signal [2], the optical address is then stored as an angular-multiplexed spectral hologram (AMSH) acting as an address bank. The address recognition is performed by optically correlating the incoming optical codes with those stored in the AMSH. Unfortunately, holographic media that respond to infrared light are unavailable. Thus, instead of the AMSH, a classical angular-multiplexed Fourier transform hologram is synthesised using a holographic plate Agfa-Gevaert 8E75 with a HeNe laser operating at a wavelength of 632.8 nm. Although the experimental verifications of 10 Gbit/s eight-chip-long address recognition show that our method can distinguish the optically encoded address, the correlation output cannot activate the optical gate switch due to the optical loss caused by the wavelength mismatch. To solve this problem, a new optical architecture for implementing IP header address recognition using second-harmonic generation (SHG) cascaded with an optical correlator is proposed. The reason for using the SHG is that the generations of second-harmonic femtosecond pulses have been widely studied [3, 4]. This will technically facilitate producing the optical code at 775 nm so that the conventional holographic media can be employed to synthesise the AMSH. In the correlation process, the use of SHG eliminates the wavelength mismatch and minimises the optical loss. Thus, activation of the optical gate by the correlator can be achieved.

Address recognition system: Fig. 1 shows a block diagram of the proposed method where the incoming optically encoded address emerges from an optical fibre and is amplified and split either to the array of optical gate switches or to the optical address recognition system. In this system, the SHG generates the second-harmonic optical address to be recognised. The holographic correlator then performs the address recognition by correlating the generated second-harmonic optical address with those stored in the AMSH. Since no wavelength mismatch occurs, the correlation output signal can activate the optical gate that routes the optical data packet to the designated address.

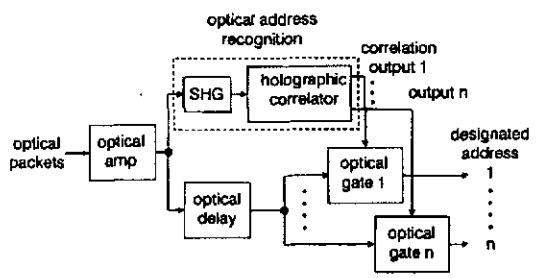

Fig. 1 *Schematic diagram of proposed method*

Synthesis of AMSH: Fig. 2 shows a schematic diagram of an optical setup for synthesising the AMSH using a modified setup of spectral holography [5]. The diffraction grating and the holographic medium are placed at, respectively, the front and the back focal planes of the Fourier transforming (FT) lens L_1. For simplicity, the SHG crystal is illustrated in a reflection scheme. In this setup we envision the use of a quasi-phase-matching (QPM) [4] technique for generating the second-harmonic optical fields $u^p_{2\omega}(t)$ and $u^r_{2\omega}(t)$ from the incoming optical packet address $u^p_\omega(t)$ and the reference pulse $u^r_\omega(t)$, respectively. They are then collimated by the collimating lenses. The QPM technique provides the use of non-birefringence materials and the elimination of constraint on polarisation. The collimated second-harmonic optical header-address and the reference pulse are set for parallel with zero relative time delay. The diffraction grating is arranged in such a way that the centre angular frequency ω_0 of the first diffraction order of the generated second-harmonic optical fields propagate along the optical axis of the system. When the resultant second-harmonic optical fields are incident on the grating at an incidence angle θ with respect to the normal of the grating, the temporal information of the optical pulses is converted into spatial information [2]. The resultant diffracted optical fields are then Fourier transformed by the FT lens L_1. The spectrally dispersed optical address and the reference pulse intersect on the holographic medium producing the spectral hologram. To synthesise the AMSH, the intersection angle of the two beams is changed by varying the incidence position of the reference pulse along the vertical direction in the grating plane.

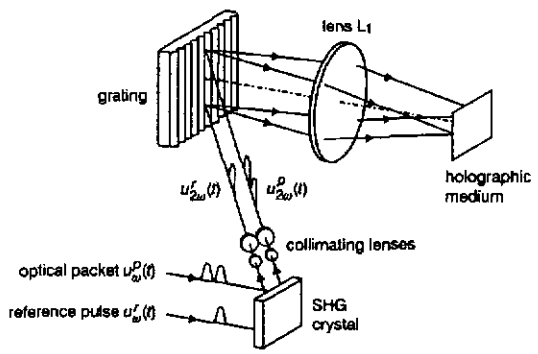

Fig. 2 *Schematic diagram of optical setup for synthesising AMSH*

Optical address recognition: The schematic diagram of the optical setup for address recognition is shown in Fig. 3. Except for the SHG crystal, the setup is similar to our previous setup [1]. The incoming second-harmonic optical code $u^i_{2\omega}(t)$ is spectrally dispersed by the combination of the grating and the FT lens L_1. Its resultant spectrum is used to read out the AMSH. When the incoming optical code matches with the corresponding code stored in the AMSH, a diffracted light is generated. Since there is no wavelength mismatch, after Fourier transformation by the lens L_2, the resultant correlation output obtained in the back focal plane of the lens can be used to activate the optical gate switch that directs the optical data packet to the designated address.

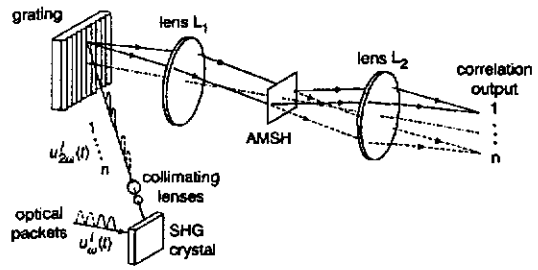

Fig. 3 *Schematic diagram of optical setup for address recognition*

System performance: The throughput performance of the method can be analysed by first assuming that the width of the chip pulse is τ and the time interval between the pulses is $\Delta\tau$. Thus, the time duration of an N-chips-long optical address is $T \simeq N(\tau + \Delta\tau)$. If the diameter of the collimated beam is X, the spatial expanse of this beam on the grating plane becomes $X\cos\theta$. Following the condition that the spatial expanse of the beam must be sufficiently larger than the spatial image of the optical address [6], we obtain

$$X\cos\theta > \lambda_0[N(\tau + \Delta\tau)]/2\pi\beta \qquad (1)$$

where λ_0 is the centre wavelength of the second-harmonic optical signal and $\beta = \lambda_0/d\omega_0$ is the dispersion parameter of the grating having a spacing of d. Equation (1) shows the required collimating size of the beam with respect to the length of the optical address.

Under coherent illumination, the total information capacity that can be processed is determined by the size of the FT lens. Since the

maximum length of the spatial image of the optical address must be equal to the half of diameter D of the FT lens [7], we obtain

$$\lambda_0[N(\tau+\Delta\tau)]/2\pi\beta = D/2 \quad (2)$$

Thus, the maximum number of chips is found to be

$$N = \frac{\pi D}{d\omega_0(\tau+\Delta\tau)} \quad (3)$$

When ω_0, τ, and $\Delta\tau$ are constants, the number of chips can be increased as the diameter of the lens becomes larger and the grating spacing is reduced. This is easily understood since the cutoff frequency of the lens is proportional to its diameter. Therefore, increasing the diameter will improve the spatial frequency response of the optical system. According to the property of the diffraction grating, the spacing governs both the incidence and the diffraction angles. For a zero degree diffraction angle, decreasing the size of the spacing leads to the increase of the incidence angle. As the result, a long temporal optical address can be projected into the spatial pattern.

Conclusions: We have proposed an IP address recognition using an optical address correlator cascaded with a second-harmonic generator. Analysis of the throughput performance of the method shows that the number of chips can be increased as the diameter of the lens becomes larger and the grating spacing is reduced.

6 April 2002
Electronics Letters Online No: 20020875
DOI: 10.1049/el:20020875

J. Widjaja (*Institute of Science, Suranaree University of Technology, Nakhon Ratchasima 30000, Thailand*)

E-mail: widjaja@ccs.sut.ac.th

References

1 WIDJAJA, J., WADA, N., ISHII, Y., and CHUJO, W.: 'Photonic packet address processor using holographic correlator', *Electron. Lett.*, 2001, **37**, (11), pp. 703–704
2 WEINER, A.M., and HERITAGE, J.P.: 'Picosecond and femtosecond Fourier pulse shape synthesis', *Rev. Phys. Appl.*, 1987, **22**, (12), pp. 1619–1628
3 WEINER, A.M., KAN'AN, A.M., and LEAIRD, D.E.: 'High efficiency blue generation by frequency doubling of femtosecond pulses in thick nonlinear crystal', *Opt. Lett.*, 1998, **23**, (19), pp. 1441–1443
4 ARBORE, M.A., FEJER, M.M., HARIHARAN, A., FERMANN, M.E., GALVANAUSKAS, A., and HARTER, D.: 'Frequency doubling of femtosecond erbium-fiber soliton lasers in periodically poled lithium niobate', *Opt. Lett.*, 1997, **22**, (1), pp. 13–15
5 WEINER, A.M., LEAIRD, D.E., REITZE, D.H., and PAEK, E.G.: 'Spectral holography of shaped femtosecond pulses', *Opt. Lett.*, 1992, **17**, (3), pp. 224–226
6 EMA, K., KAGI, N., and SHIMIZU, F.: 'Optical compression using a monochromator and a concave mirror', *Opt. Commun.*, 1989, **71**, (1,2), pp. 103–106
7 VANDERLUGT, A.: 'Optical signal processing' (Wiley, New York, 1992) pp. 128–130

Record tuning range of InP-based multiple air-gap MOEMS filter

J. Daleiden, V. Rangelov, S. Irmer, F. Römer, M. Strassner, C. Prott, A. Tarraf and H. Hillmer

Continuously tunable Fabry-Perot filters based on multiple InP/air-gap MOEMS technology are presented. Record wavelength tuning >112 nm with an actuation voltage of only 5 V is demonstrated. The FWHM remains constant over the entire tuning range. The stopband covers both the second and third optical telecommunication window (1250–1800 nm).

Introduction: Optical filters with a wide and continuous tuning range are very attractive components for flexible dense wavelength division multiplex (DWDM) networks [1]. Fabry-Perot filters based on micro-optoelectromechanical system (MOEMS) technology have been reported for various material systems [2–7]. Up to now the wavelength tuning range of these devices was approximately 70 nm, limited by the mechanical flexibility of the tunable membrane and the effective optical cavity length. The control of the material strain has been a technological barrier for the realisation of flexible thin and flat membranes [8], being essential for high tunability. To overcome this problem, thicker membranes (>1 μm) have been chosen and/or significant tensile strain has been applied. Both approaches have resulted in reduced mechanical tuning efficiencies and high actuation voltages between 14 and 40 V for 70 nm spectral tuning [2–7].

Design of device: In our design we applied an InP/air-gap technology with well controlled material strain [9], facilitating extremely flexible (3/4) λ (357 nm, $\lambda_{air} = 1500$ nm) thick InP membranes. At the same time the optical performance is improved. Owing to the very high refractive index contrast between InP ($n = 3.17$) and air ($n = 1$) a wide stopband of 550 nm spectral width (1250–1800 nm) and a short effective cavity length (1.3λ) are possible. The calculated free spectral range of the devices is 632 nm.

Fig. 1 is a schematic diagram showing the cross-section of the device. The simple vertical structure comprises six suspended InP membranes (each 357 nm thick). The upper three InP membranes are separated by $\lambda/4$ (375 nm) air-gaps and act as the top distributed Bragg reflector (DBR). Analogous, the three lower InP membranes define the second DBR. The air-gap between top and bottom DBR is 815 nm thick and acts as the cavity. The simulated cavity resonance is at 1563 nm. The centre wavelength of the DBRs is $\lambda = 1500$ nm. This is two reasons: (i) the filter is able to block both the second and the third optical telecommunication window (calculated reflectivity at 1300 nm is 99.6%); (ii) the optimum performance of the filter is obtained in the centre of the expected tuning range (120 nm).

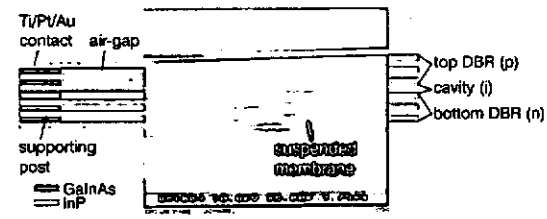

Fig. 1 *Cross-sectional view of six air-gap filter. Includes scanning electron micrograph*

The membranes are circularly shaped (40 μm diameter) and supported by three (design 1) or four (design 2) 10 μm wide suspensions (Fig. 2). The length of the suspensions varies between 10 and 80 μm. They are connected to three or four square shaped supporting posts (150 × 150 μm^2), respectively.

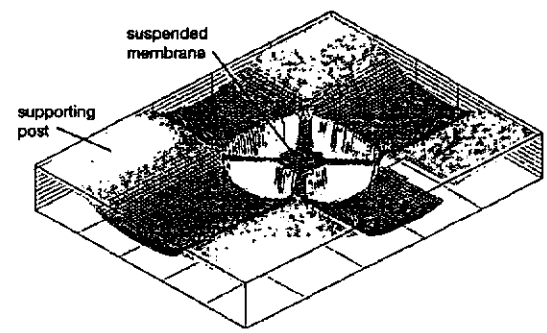

Fig. 2 *White light interferometric measurement (Zygo LOT) of filter with four suspensions*

Fabrication: The InP/GaInAs multiple-layer structure is grown on n-type InP substrate by metal organic vapour phase epitaxy (MOVPE). The top DBR is p-doped (10^{17} cm^{-3}) whereas the bottom DBR is n-doped (10^{17} cm^{-3}). An intrinsic GaInAs (815 nm thick) layer defines the filter cavity. After removing the top InP layer in the area where the contact is formed, the p-ohmic contact